

Journal of Materials Chemistry A

Accepted Manuscript



This is an *Accepted Manuscript*, which has been through the Royal Society of Chemistry peer review process and has been accepted for publication.

Accepted Manuscripts are published online shortly after acceptance, before technical editing, formatting and proof reading. Using this free service, authors can make their results available to the community, in citable form, before we publish the edited article. We will replace this *Accepted Manuscript* with the edited and formatted *Advance Article* as soon as it is available.

You can find more information about *Accepted Manuscripts* in the [Information for Authors](#).

Please note that technical editing may introduce minor changes to the text and/or graphics, which may alter content. The journal's standard [Terms & Conditions](#) and the [Ethical guidelines](#) still apply. In no event shall the Royal Society of Chemistry be held responsible for any errors or omissions in this *Accepted Manuscript* or any consequences arising from the use of any information it contains.

Magnetic carbon nanofibers containing uniformly dispersed Fe/Co/Ni nanoparticles as stable and high-performance electromagnetic wave absorbers

Cite this: DOI: 10.1039/x0xx00000x

Received 00th January 2012,
Accepted 00th January 2012

DOI: 10.1039/x0xx00000x

www.rsc.org/

Jun Xiang,^{*a} Jiale Li,^a Xionghui Zhang,^a Qin Ye,^a Jiahuan Xu^a
and Xiangqian Shen^b

The carbon nanofibers with ferromagnetic metal nanoparticles (CNFs-*M*, *M* = Fe, Co, and Ni) have been synthesized by carbonizing electrospun polyacrylonitrile nanofibers including metal acetylacetonate in argon atmosphere, and their phase composition, microstructure, magnetic properties and electromagnetic (EM)-wave absorptability have been studied. The microstructure analysis shows that the in-situ formed metal nanoparticles are well distributed along carbon-based nanofibers and encapsulated by ordered graphite layers. The investigation of magnetic properties and EM-wave absorptability reveals that the as-synthesized CNFs-*M* have typical characteristics of ferromagnetic materials and exhibit excellent EM-wave absorption properties (reflection loss exceeding -20 dB) from C-band to Ku-band (4–18 GHz) over the absorber thickness of 1.1–5.0 mm due to the efficient complementarities of the complex permeability and permittivity resulting from the magnetic metal nanoparticles and lightweight carbon, as well as the particular particle/graphite core/shell microstructures in CNFs-*M*. Moreover, a minimum reflection loss value of -67.5, -63.1, and -61.0 dB is achieved at 16.6, 12.9, and 13.1 GHz with a matching thickness of 1.3, 1.6, and 1.7 mm for CNFs-Fe, CNFs-Co, and CNFs-Ni, respectively. These magnetic carbon nanofibers are attractive candidates for the new type of high performance EM-wave absorbing materials.

Introduction

The absorption and interference shielding of electromagnetic (EM) wave have been very important issues in both civil and military fields.^{1–4} In order to solve the EM interference and stealth problems, much effort has been devoted in recent years to the development of high-performance EM wave absorption materials with wide frequency band, strong absorption, light weight, and thin thickness. It is well known that the relative complex permittivity ($\epsilon_r = \epsilon' - j\epsilon''$) and permeability ($\mu_r = \mu' - j\mu''$) of the absorbers are main factors determining the microwave absorption properties.^{5,6} The balance of the permittivity and permeability, so-called the EM impedance matching, is critical for the improvement of EM-wave absorption.⁷ According to dissipation mechanism, EM wave absorption materials can be categorized into two types: dielectric loss and magnetic loss.^{8,9} It is hard to attain impedance matching condition $Z_{in} = Z_0(\mu_r/\epsilon_r)^{1/2}$ for unilateral dielectric loss or magnetic loss materials.⁵ The combination of magnetic and dielectric materials has been considered as an effective way to reach the impedance matching and in turn to achieve an excellent EM absorption due to the synergistic effect on dissipation of EM wave energy.^{9,10} Accordingly, some highly-effective absorbers, for instance, by compositing magnetic loss nanoparticles and dielectric loss components such as graphene,^{7,11,12} carbon onions,^{1,13} carbon nanotubes (CNTs)^{6,10,14} and carbon nanofibers (CNFs)^{2,8,15} have been developed.

Among a variety of dielectric absorbers, carbon fibers have attracted considerable attention because of their lightweight, large aspect ratio, high strength, good conductivity, thermal and chemical stability, and low manufacturing cost.^{8,9,15,16} In previous reports, many treatments have been used to enhance the microwave absorption performance of carbon fibers, including reducing the carbonization temperature, surface modification and changing the cross sectional shape of carbon fibers.^{17,18} Specifically, coating the carbon fibers with a layer of magnetic metal,^{15,19,20} ferrites^{18,21} or oxides^{17,22} have been found not only to significantly enhance the microwave absorption properties due to the optimization of EM parameters, but also to effectively lower the entanglement between fibers and improve the dispersion characteristics in the polymer matrix. In the reported techniques used to prepare one-dimensional nanomaterials including nanofibers, nanobelts, nanotubes and nanowires, electrospinning is a straightforward and cost-effective method for large-scale fabrication of fibers with diameters from nanometer to micron.^{23–25} Generally, the synthesis process of magnetic metal/carbon composite nanofibers by electrospinning consists of three steps. First, there is the preparation of electrospun metal precursor/polymer nanofiber mats. Then, the nanofiber mats are calcined at high temperature in air. Finally, the metal/carbon composite nanofibers are obtained by reduction treatment.²⁵ In order to simplify the procedure and reduce the production cost, a two-step method has been exploited to fabricate metal/carbon nanofibers, in

which the as-electrospun nanofibers were calcined directly in argon atmosphere. This method is safe, economical, and more effective. In recent years, some magnetic metal/carbon hybrid nanofibers have been successfully prepared by this alternative two-step electrospinning strategy and their electric, magnetic, optical and electrochemical properties have been investigated.^{26–29} However, there are few studies on the EM-wave absorption properties of such magnetic CNFs so far. Recently, Zhang and co-workers⁸ prepared magnetic CNFs loaded with Fe₃O₄ nanoparticles by electrospinning combined with stabilization and carbonization treatment and evaluated their microwave absorbing properties. Their results showed that the minimum reflection loss reached about –45 dB for a 5 mm absorber layer with 5 wt% carbon/Fe₃O₄ composite nanofibers. In comparison with the traditional ferrite absorbers, the metallic soft magnetic materials (e.g., Fe, Co, Ni, and their alloys) have a larger saturation magnetization value and a higher Snoek's limit,^{30,31} which are good for improving the EM wave absorption performances. Therefore, it is reasonable to speculate that if metal soft magnetic nanoparticles are encapsulated in the CNFs, a further enhancement in properties, such as a stronger absorption and a thinner matching thickness may be obtained. Besides, it is important to note that a good physical and chemical stability can be anticipated for such magnetic carbon hybrid nanofibers due to the protection of carbon.

In the present work, the carbon nanofibers containing uniformly dispersed ferromagnetic metal nanoparticles (CNFs-*M*, *M* = Fe, Co, and Ni) have been synthesized using the two-step electrospinning method and their EM wave absorption properties are evaluated. These hybrid nanofibers display superior EM absorption performances at a lower mass density and a smaller absorber layer as compared to many earlier reported magnetic carbon hybrid nanocomposites, highlighting the important of their applications in the EM-wave absorbing filed.

Experimental

Sample preparation

CNFs-*M* (*M* = Fe, Co, and Ni) were prepared by electrospinning and subsequent heat treatment. In a typical procedure, 0.9 g of PAN (*M_w* = 150000, Aldrich Co.) was mixed with 8.3 g of dimethylformamide (DMF) in a small bottle, followed by magnetic stirring in water bath at 50 °C for 3 h to ensure the dissolution of PAN. 0.8 g of metal acetylacetonate (metal = Fe, Co, or Ni) was then added to the PAN/DMF solution and continuously stirred for about 12 h at room temperature. Using the electrospinning apparatus with the applied DC voltage of 15 kV, receiving distance of 20 cm and solution feed rate of 0.5 mL/h, the obtained solutions were electrospun into PAN precursor nanofibers that contained the corresponding metal acetylacetonate. The collected precursor nanofibers were stabilized at 250 °C for 3 h in air followed by carbonization in a tube oven at 1000 °C, 1100 °C or 1200 °C for 1 h under a high-purity argon atmosphere to respectively produce CNFs-Fe, CNFs-Co, and CNFs-Ni. For comparison, the pure CNFs were also prepared using the same synthesis route with a carbonization temperature of 1000 °C.

Characterization

Phase analysis of the as-synthesized products was performed by powder X-ray diffraction (XRD) on a Rigaku D/max-2500PC diffractometer at a voltage of 40 kV and a current of 200 mA with graphite monochromatized Cu K α (λ = 0.154056 nm) radiation. The surface morphology and chemical composition of the samples were characterized by a JEOL JSM-7001F field-emission scanning electron microscopy (FESEM) equipped

with energy-dispersive X-ray analysis (EDX, Oxford Instrument). The microstructure of the nanofibers was analyzed using a JEOL JEM-2100 transmission electron microscopy (TEM) operating at 200 kV accelerating voltage. The room temperature magnetic properties were investigated by a HH-20 vibration sample magnetometer (VSM) with an applied external field of 1.5 T. Raman spectra of randomly oriented samples were recorded on a ThermoFisher DXR Raman spectrometer with a 532 nm laser. The composite samples used for EM properties measurement were prepared by uniformly mixing these magnetic carbon nanofibers in a silicone matrix with a mass fraction of 5%. For the fabrication of the testing samples, the required amount of CNFs-*M*, silicone and corresponding curing agent (Dow Corning Sylgard 184) were mixed together and sufficiently stirred for about 1 h at room temperature to produce a homogeneous mixture of a desired composition. The mixture was filled into a stainless steel mold and then cured in a vacuum oven at 100 °C for 2 h to form a toroidal-shaped specimen with an outer diameter of 7.00 mm, an inner diameter of 3.04 mm and a thickness of 2.00 mm. The complex permeability (μ_c) and permittivity (ϵ_r) of the silicone composites with 5 wt% of CNFs-*M* were measured in the 1–18 GHz range by using an Agilent E5071C vector network analyzer.

Results and Discussion

Phase, morphology and microstructure

The phase composition and structure of the as-synthesized CNFs-*M* and pure CNFs were examined by powder XRD and the recorded patterns are presented in Fig. 1. For the pure CNFs, there is only a dispersive peak structure in the XRD pattern, suggesting that the sample is mainly composed of amorphous carbon.^{9,32} For the CNFs-*M*, a broad diffraction peak at 2θ of around 26° can be indexed to (002) crystal plane of hexagonal graphite (JCPDS No. 41-1487). This indicates that the amorphous carbon comprising these nanofibers has been partially transformed into the graphite-like carbon. The (002) interplanar spacing values of CNFs-Fe, CNFs-Co, and CNFs-Ni are calculated to be 0.3395, 0.3457, and 0.3420 nm, respectively. Both the *d*-spacing and the intensity of (002) peak seem to show that the carbon in CNFs-Fe should have the highest degree of crystalline and graphitization among the three samples.^{32,33} Meanwhile, for CNFs-Co and CNFs-Ni, all of the other diffraction peaks in the patterns can be respectively ascribed to the well-crystallized cobalt (JCPDS No. 15-0806) or nickel (JCPDS No. 04-0850) metals with a face-centered cubic (fcc) structure. The formation of metal phase should be mainly due to the presence of carbon derived from the decomposition of PAN during the carbonization process, which can reduce the related metal oxides to metal at elevated temperatures.²⁸ Simultaneously, the presence of metal phase also enhances the PAN graphitization process upon calcination in argon atmosphere.²⁶ The above results demonstrate that the as-prepared CNFs-Co and CNFs-Ni are composed of amorphous carbon, graphite and metal phases. No other phases corresponding to oxides or carbides are found herein, indicating an effective protection of carbon matrix to metal nanoparticles within the nanofibers. However, in the case of CNFs-Fe, except the diffraction peaks from the body-centered cubic (bcc) phase of Fe (JCPDS No. 87-0721), there are also some clear peaks of Fe₃O₄ in the pattern,⁸ implying that the complete phase transformation cannot be achieved in carbonization process and the final product still contains a certain amount of Fe₃O₄. In

addition, the n-diamond phase is detected in the CNFs-Fe nanocomposite, which has also been reported by other studies.^{6,34} Based on the XRD data, the average crystallite sizes of Fe, Co, and Ni nanoparticles can be estimated from Scherrer's formula to be about 19.1, 62.3, and 33.6 nm for CNFs-Fe, CNFs-Co, and CNFs-Ni, respectively. The information about the structure of the carbon in CNFs-*M* is further investigated from Raman spectra, and the results are shown in Fig. 2. The Raman spectra of all samples show two main broad peaks centered at about 1341 and 1574 cm^{-1} which respectively correspond to D-band from amorphous carbon and G-band from graphite carbon.^{6,25,33} Thus, the intensity ratio of the D- and G-band ($I_{\text{D-band}}/I_{\text{G-band}}$) is indicative of the degree of graphitization. The ratio values for CNFs-Fe, CNFs-Co, and CNFs-Ni are 0.64, 0.94, and 0.72, respectively. This indicates that the degree of graphitization of the carbon within CNFs-*M* increases in the order of CNFs-Co < CNFs-Ni < CNFs-Fe. In other words, CNFs-Fe sample has the highest degree of graphitization, which is consistent with the XRD results.

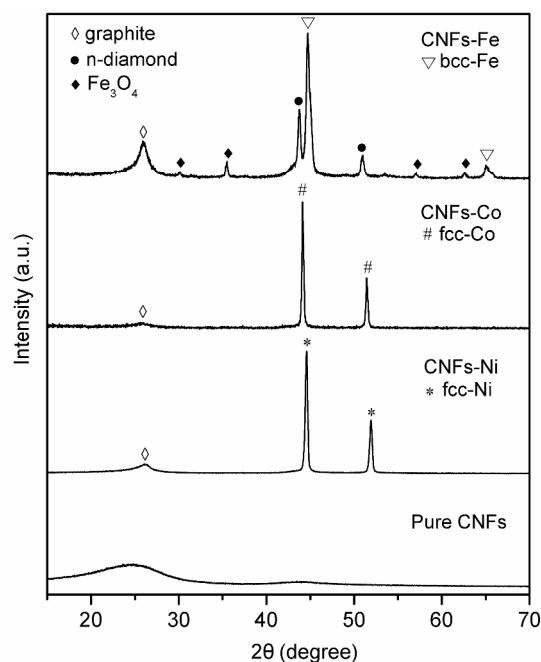


Fig. 1 XRD patterns of the as-synthesized CNFs-Fe, CNFs-Co, and CNFs-Ni.

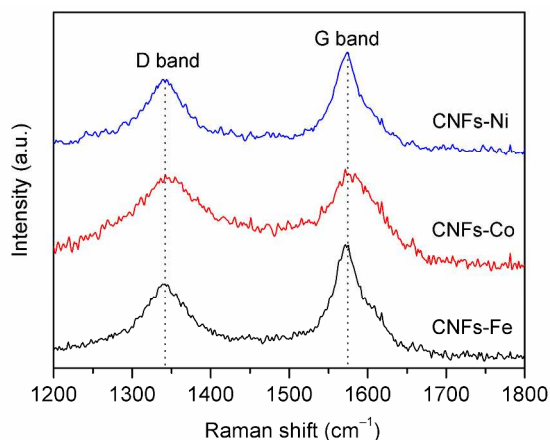


Fig. 2 Raman spectra of CNFs-Fe, CNFs-Co, and CNFs-Ni.

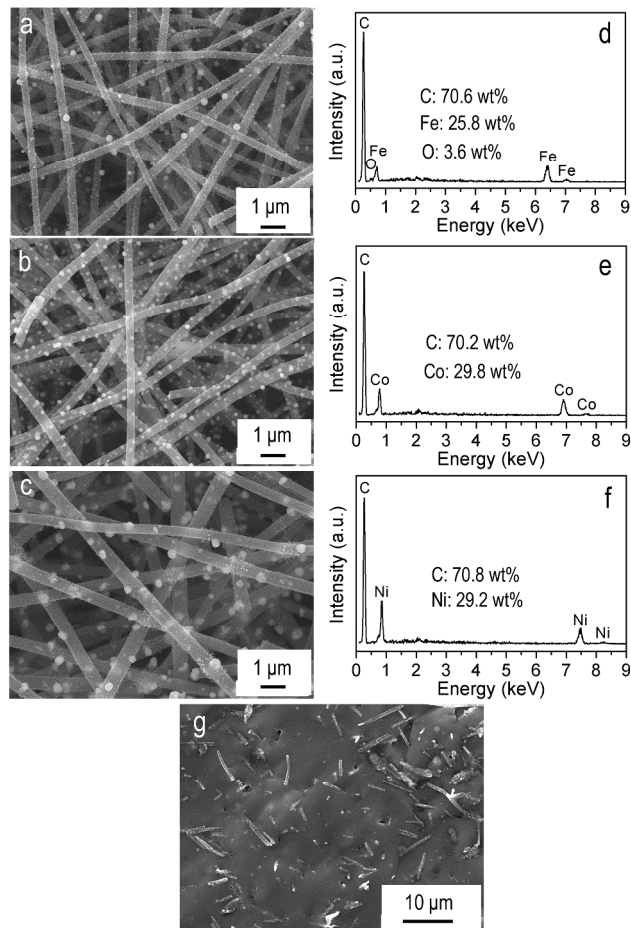


Fig. 3 (a–c) FESEM images and (d–f) EDX spectra of the prepared composite nanofibers: (a and d) CNFs-Fe, (b and e) CNFs-Co, (c and f) CNFs-Ni. (g) Cross-section FESEM images of silicone composites with 5 wt% composite nanofibers.

Fig. 3a–c shows the representative FESEM images of the synthesized CNFs-Fe, CNFs-Co, and CNFs-Ni. It can be clearly seen that the well-defined fibrous morphology is perfectly maintained for the three samples after carbonization at high temperature, and each individual nanofiber is uniform in cross-section. In addition, some short nanoprotusions are observed on the fiber surface. The lengths of these nanofibers can reach a millimeter to centimeter scale and the average diameters are 290 ± 34 , 345 ± 42 , and 475 ± 65 nm for CNFs-Fe, CNFs-Co, and CNFs-Ni, respectively. Their chemical compositions are characterized using EDX and shown in Fig. 3d–f, respectively. The experimental results show that there are only C and related metal elements existing in CNFs-Co and CNFs-Ni, and the Co and Ni mass fractions are respectively 29.8% and 29.2%. While for the CNFs-Fe sample, a weak peak coming from O element can be observed except for Fe and C peaks in the corresponding EDX spectrum. It indicates that the CNFs-Fe contains some iron oxides, which is in good agreement with the XRD results. The Fe content in CNFs-Fe nanocomposite is calculated by excluding the content of Fe_3O_4 to be about 16.4 wt% based on the EDX result. Fig. 3g presents a cross section FESEM image of silicone composites with 5 wt% CNFs-*M*. We can see that the magnetic carbon composite nanofibers are well dispersed in the silicone matrix.

On the same samples presented above, a conventional TEM study has been conducted to further investigate their microstructures and the distribution of metal nanoparticles in the corresponding nanofibers. Fig. 4a–c shows typical TEM images of single CNFs-Fe, CNFs-Co and CNFs-Ni composite nanofibers, respectively. As observed, the in-situ formed Fe/Co/Ni nanoparticles are roughly spherical and well distributed along the nanofibers. Meanwhile, these Fe/Co/Ni nanoparticles display a broad size distribution and the mean particle sizes obtained by measuring more than 100 particles are around 17, 155 and 110 nm, respectively. For CNFs-Co and CNFs-Ni, the particle sizes of Co and Ni nanoparticles are much larger than the corresponding crystallite sizes estimated by the XRD data, indicating that most of the Co and Ni nanoparticles inside the nanofibers are polycrystalline aggregates. Further structural characterization for these metal particles was carried out by selected area electron diffraction (SAED) and high-resolution TEM (HRTEM). The insets of Fig. 4a–c show the SAED patterns from a single Fe, Co, and Ni nanoparticles in CNFs-*M*. These SAED patterns not only further confirm the existence of bcc-Fe, fcc-Co, and fcc-Ni in the samples but also demonstrate the Co and Ni nanoparticles both are polycrystalline. As shown in Fig. 4d–e, the HRTEM images reveal that these metal nanoparticles are basically parceled by ordered graphite layers, similar to particles/graphite core/shell nanocapsules in microstructures. The formation of graphite around the particles should be attributed to the good catalytic graphitization effect of these metals as reported earlier by

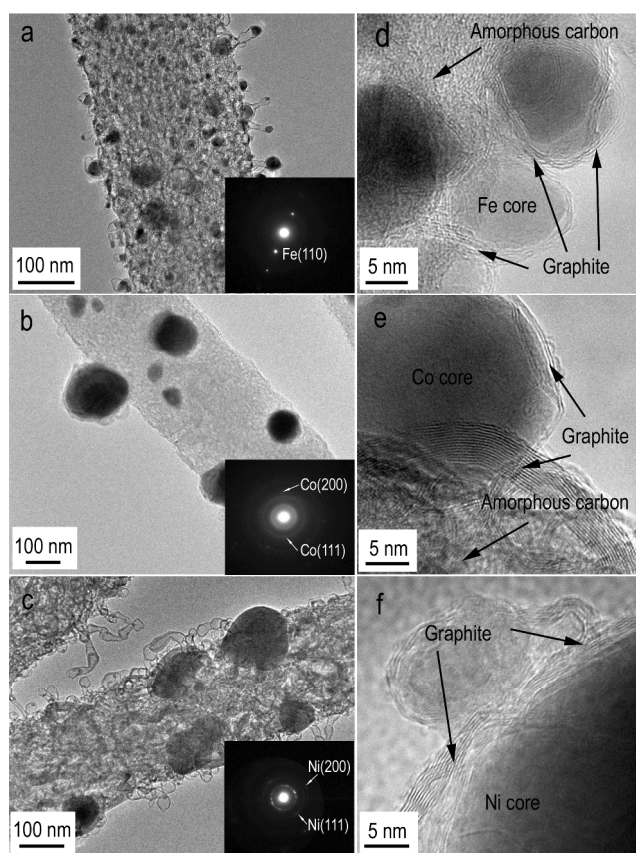


Fig. 4 (a–c) TEM and (d–f) high-resolution TEM images of the synthesized composite nanofibers: (a and d) CNFs-Fe, (b and e) CNFs-Co, (c and f) CNFs-Ni. Insets in (a)–(c) are the SAED patterns of a single Fe, Co, and Ni nanoparticles.

others.^{27,35} Furthermore, the TEM images also further confirm the coexistence of disordered carbon and graphite phases in these samples. It is noteworthy that the electromagnetic properties of such CNFs/particles nanocomposites will benefit from this uniform dispersion and particular core/shell microstructure because they can construct the good electromagnetic match in nanoscaled geometry.^{31,36}

Magnetic properties

Fig. 5 shows the magnetic hysteresis loops (M – H loops) combined with the expanded low-field hysteresis curves (inset of Fig. 5) of CNFs-Fe, CNFs-Co, and CNFs-Ni measured at room-temperature, which indicate the magnetic properties, including saturation magnetization M_s and coercivities H_c , respectively. As can be seen, the three samples exhibit typical soft ferromagnetism and their magnetizations reach saturation with the external field of about 15 kOe. The M_s values of CNFs-Fe, CNFs-Co, and CNFs-Ni are about 64.2, 40.5, and 18.6 emu/g, respectively, which are significantly lower than the values of bulk Fe (221.71 emu/g), Co (162.55 emu/g), and Ni (58.57 emu/g).³⁷ The decrease in the magnetization is mainly attributed to the existence of nonmagnetic carbon component in nanofibers.^{25,31} Moreover, the large specific area and the imperfection of the crystalline structure at the surface may also lead to a significant decrease in the nanofiber saturation magnetization.²⁶ The CNFs-Fe has the largest saturation magnetization among the three samples, which is beneficial for high permeability. On the other hand, the inset of Fig. 5 clearly indicates that the synthesized composite nanofibers exhibit great enhanced coercivities as compared to the corresponding bulk metal materials. The H_c values obtained in CNFs-Fe, CNFs-Co, and CNFs-Ni are round 107.6, 239.6, and 81.4 Oe; whereas those of bulk Fe, Co, and Ni are only 1, 10, and 0.7 Oe,³⁷ respectively. Commonly, magnetic nanomaterials have a larger coercivity than corresponding bulk materials due mainly to the considerable increase of surface anisotropy filed induced by the small size effect.

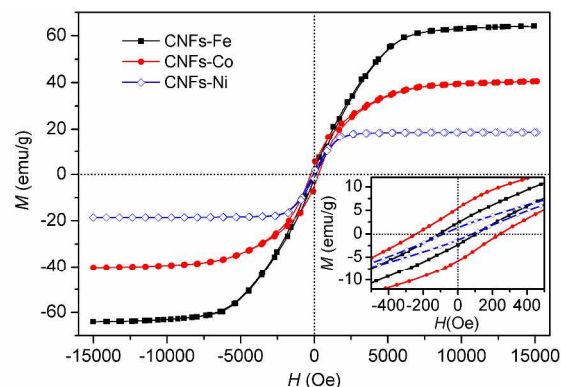


Fig. 5 Magnetic hysteresis loops of CNFs-Fe, CNFs-Co, and CNFs-Ni at room temperature. Inset is expanded low field hysteresis curves.

Electromagnetic characteristics

The electromagnetic parameters (relative complex permittivity, $\epsilon_r = \epsilon' - j\epsilon''$ and relative complex permeability ($\mu_r = \mu' - j\mu''$) of the silicone composites containing 5 wt% of CNFs-Fe, CNFs-Co, and CNFs-Ni as fillers, respectively, were measured in the frequency range of 1–18 GHz at room temperature for the investigation of EM absorption properties. Fig. 6 shows the

frequency dependence of the real part (ϵ') and imaginary part (ϵ'') of relative complex permittivity measured for the three samples. It can be found that the ϵ' values decline from 16.2, 17.2, and 14.6 to 11.6, 11.7, and 11.3 while the ϵ'' values increase from 2.1, 2.3, and 1.5 to 6.7, 7.1, and 4.8 for CNFs-Fe, CNFs-Co, and CNFs-Ni, respectively, over the 1–18 GHz frequency range. Compared with the CNFs-Co and CNFs-Ni, the CNFs-Fe exhibits an obvious peak in the ϵ'' curve over the 10.5–16.6 GHz frequency range, indicating a dielectric resonance behavior. As we know, the real permittivity is related to the polarization, while the imaginary permittivity implies the dielectric loss. For the present three samples, their complex permittivity values, especially for imaginary parts, are lower than or comparable to those of porous graphitic carbons encapsulating Fe nanoparticles ($\epsilon'' = 120\text{--}60$),⁹ Fe-Co alloy coated carbon fibers ($\epsilon'' = 9.7\text{--}4.3$),²⁰ carbon-coated nickel nanocapsules ($\epsilon'' = 7.2\text{--}3.7$),³¹ Fe/CNFs ($\epsilon'' = 90\text{--}40$) and carbon-coated Fe composites ($\epsilon'' = 50\text{--}45$).³⁸ It suggests that the prepared CNFs-Fe, CNFs-Co, and CNFs-Ni nanocomposites have a relatively weak dielectric loss against EM wave. According to the free electron theory,³⁹ $\epsilon'' \approx 1/2\pi\epsilon_0\rho f$, where ρ is the resistivity. It can be speculated that the lower ϵ'' values indicate a higher electric resistivity with respect to the aforementioned magnetic carbon hybrid nanocomposites. The higher electric resistivity may result from the few point defects existing in these composite nanofibers, the effective dispersion, as well as the particular particle/graphite core/shell microstructures.^{31,40} In general, a proper electric resistivity and proper dielectric loss are favourable to the improvement of the EM wave absorption performance.

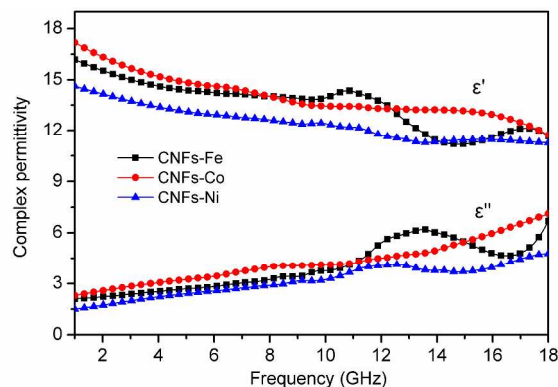


Fig. 6 Frequency dependence of the complex permittivity of the CNFs-*M*/silicone composites.

The real part (μ') and imaginary part (μ'') of relative complex permeability are plotted as a function of frequency in Fig. 7. As can be seen, the three samples show a similar dispersive behavior and the differences between permeability values are small. The μ' values vary in the range of 1.21–1.00, 1.12–0.96, and 1.15–0.98 with slight fluctuations at frequency region over 1–18 GHz for CNFs-Fe, CNFs-Co, and CNFs-Ni, respectively, while the corresponding μ'' values are close to 0. These very low permeability values in the present systems should be attributed to the trace amount of magnetic Fe/Co/Ni nanoparticles and also the Snoek limit at high frequencies. Nevertheless, for the imaginary part of complex permeability of composites, especially CNFs-Fe composite, two small resonance peaks can be observed respectively in the low-frequency and high-frequency regions. In general, the magnetic loss of magnetic materials originates mainly from eddy current

loss, natural resonance, and exchange resonance in the microwave region.^{6,25} The eddy current loss is related to the thickness (d) and the electric conductivity (σ) of the composites, which can be expressed by $\mu''(\mu')^{-2}f^{-1} = 2\pi\mu_0d^2\sigma$, where μ_0 is the permeability of vacuum. If the observed magnetic loss only results from eddy-current loss, the values of $\mu''(\mu')^{-2}f^{-1}$ should be a constant when frequency varies. However, Fig. 8 shows that above situation does not exist for the present CNFs-Fe, CNFs-Co, and CNFs-Ni systems because their $\mu''(\mu')^{-2}f^{-1}$ values present a decreasing trend generally with increasing frequency in the 1–18 GHz range. Therefore, the eddy current loss can be precluded. The natural resonance frequency can be calculated by the equation: $f = \gamma H_k$,⁴¹ where f is the resonance frequency, γ the gyromagnetic ratio, H_k the anisotropy field. Considering that the magnetocrystalline anisotropy field of bcc-Fe, fcc-Co, and fcc-Ni is 600, 500, and 130 Oe,⁶ the calculated natural resonance frequency is 1.8, 1.5, and 0.39 GHz, respectively. These values are smaller than the frequency of the measured resonance peak at the low-frequency region, which may be attributed to the surface and shape anisotropy of magnetic Fe/Co/Ni nanoparticles.²⁵ Moreover, the resonance at the high-frequency range may be due to the exchange resonance according to Aharoni's theory which has been reported in previous reports.⁴²

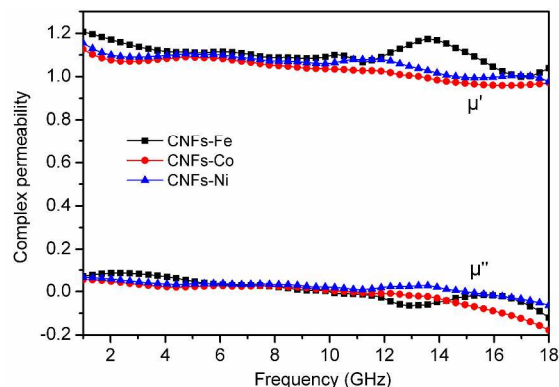


Fig. 7 Frequency dependence of the complex permeability of the CNFs-*M*/silicone composites.

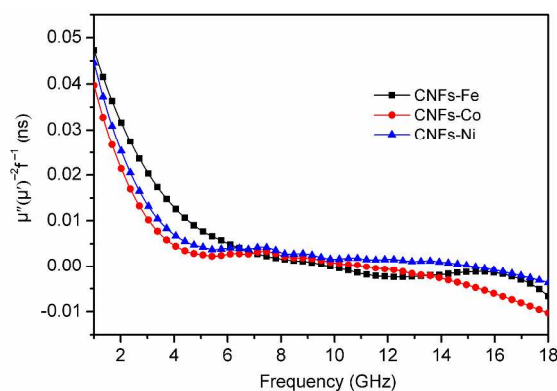


Fig. 8 Values of $\mu''(\mu')^{-2}f^{-1}$ for the CNFs-*M*/silicone composites versus frequency

It is worthy to note that the imaginary permeability of these three samples presents negative values at the high-frequency range (about 11–18 GHz). This phenomena related to negative permeability have been reported in many composites containing fillers such as MWCNTs,⁴³ porous carbon,⁴⁴ graphene,⁷

Fe₃O₄/ZnO core/shell nanorods,⁴⁵ carbon microtube/Fe₃O₄ nanocomposites,³ and Fe-Co alloy coated CNFs.²⁰ The Physical mechanisms of such permeability have been researched both experimentally and theoretically.

Dielectric loss and magnetic loss are the two possible contributions to EM-wave absorption.⁴⁰ In order to investigate which one is dominate for the CNFs-Fe, CNFs-Co, and CNFs-Ni nanocomposites, the dielectric loss tangent ($\tan \delta_e = \epsilon''/\epsilon'$) and the magnetic loss tangent ($\tan \delta_m = \mu''/\mu'$) are calculated and shown in Fig. 9. For the three samples, a generally increasing and declining tendency can be observed for the dielectric and magnetic loss with the increase of frequency, respectively. The values of $\tan \delta_e$ and $\tan \delta_m$ vary respectively in the range of 0.104 to 0.720 and 0.074 to -0.186. The appearance of the negative magnetic loss tangent at the high-frequency region is due to the negative permeability. In the entire frequency range, the value of $\tan \delta_e$ is much larger than that of $\tan \delta_m$, which suggests the dielectric loss plays a main role in the intrinsic EM absorptions of these samples. The similar phenomenon has also been reported in other magnetic carbon hybrid absorbing materials, e.g., FeCo@C nanocapsules,¹ MWCNTs/Fe/Co/Ni nanopowders,⁶ CoNi@C nanocapsules,¹³ Fe-Co alloy coated CNFs,²⁰ and Fe₃O₄ coated CNFs.²¹ It is known that the absorption of EM energy by dielectrics are mainly arises from the dipole polarization and the interfacial polarization at microwave frequency.^{44,46,47} In our case, the number of surface atoms with unsaturated bonds in Fe/Co/Ni particles will greatly increase as their sizes are in nanoscale, resulting in an increase of the dipoles. Consequently, the more dipole polarization can contribute to the dielectric loss. Furthermore, the fine dispersion of Fe/Co/Ni nanoparticles in carbon-based nanofibers can introduce more extra interfaces and as a result the interfacial polarization and the associated relaxation occurred at the nanoparticles/carbon interfaces will be stronger, which also contribute to the dielectric loss.⁴⁸ In addition, the space-charge polarization, which occurs between adjacent metal nanoparticles, possibly contributes extra relaxation process and results in the increase of the dielectric loss in some degree.⁴⁰

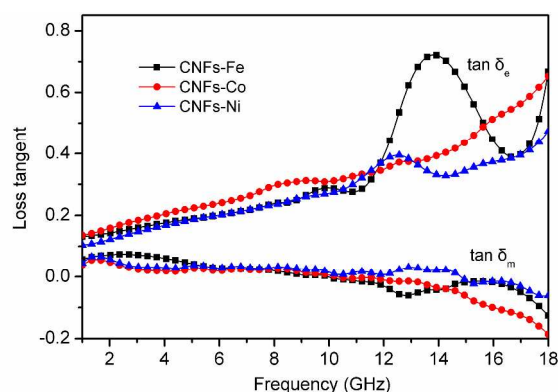


Fig. 9 Frequency dependence of dielectric loss and magnetic loss tangent of the CNFs-*M*/silicone composites.

EM-wave attenuation in the interior of absorber is one of key factors for an excellent absorber. The attenuation constant α determines the attenuation properties of materials. According to transmission line theory and EM-wave propagation constant, the α can be expressed by

$$\alpha = \frac{\sqrt{2\pi f}}{c} \times \sqrt{(\mu''\epsilon'' - \mu'\epsilon') + \sqrt{(\mu''\epsilon'' - \mu'\epsilon')^2 + (\epsilon'\mu'' + \epsilon''\mu')^2}} \quad (1)$$

where f is the frequency of EM-wave and c is the velocity of light.⁴⁰ As shown in Fig. 10, the dependence of α on frequency shows that the CNFs/Fe has the maximum α value among the three samples in most of the tested frequency range, especially at the high-frequency range. Therefore, it can be speculated that the CNFs-Fe may exhibit better EM-absorption properties than the CNFs-Co and CNFs-Ni samples.

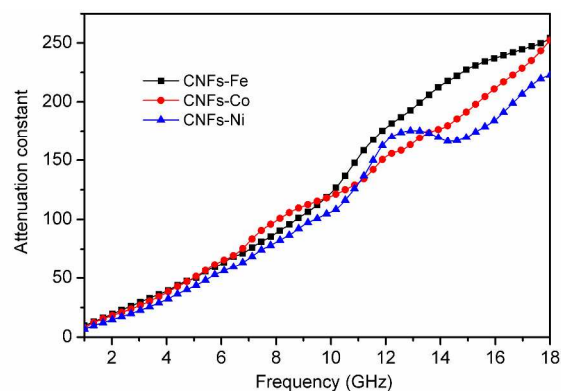


Fig. 10 Attenuation constant of the CNFs-*M*/silicone composites as a function of frequency.

EM-wave absorption properties

To reveal the EM-wave absorption properties of the as-synthesized samples, the reflection loss (RL) values of the CNFs-Fe, CNFs-Co, and CNFs-Ni nanofiber composites were calculated using the measured relative complex permeability (μ_r) and permittivity (ϵ_r) at thickness from 1.1 to 5.0 mm and frequency from 1 to 18 GHz according to the following equations^{25,30}

$$Z_{in} = Z_0 (\mu_r / \epsilon_r)^{1/2} \tanh \left[j(2\pi f d / c) (\mu_r \epsilon_r)^{1/2} \right] \quad (2)$$

$$RL(\text{dB}) = 20 \lg |(Z_{in} - Z_0) / (Z_{in} + Z_0)| \quad (3)$$

where Z_{in} is the input impedance of the absorber, Z_0 is the impedance of air, c is the velocity of light, f is the frequency of microwaves, and d is the thickness of the absorber. The results are shown in Fig. 11a-c. At a given thickness, a RL peak appears at a frequency. The RL peaks exceeding -20 dB are achieved at all thicknesses tested. An RL value below -20 dB means that more than 99% of the incident EM-wave is absorbed, which is a typical target to be attained for the EM-wave absorbers from a practical application point of view.^{40,49} The absorption bandwidths with the RL less than -20 dB are up to 14.7 GHz (from 3.3 to 18 GHz) for CNFs-Fe, 14.5 GHz (from 3.5 to 18 GHz) for CNFs-Co, and 14.2 GHz (from 3.8 to 18 GHz) for CNFs-Ni, when the absorber thickness is between 1.1 and 5.0 mm. The above results demonstrate that these three samples have excellent EM-wave absorption performances from C-band to Ku-band. This frequency ranges covers the absorption frequency range of the traditional ferrite absorbers³⁰ and many earlier reported nanocomposites.^{1,3,6,8,10-22} Moreover, the minimum RL values of -67.5, 63.1, and 61.0 dB are obtained at 16.6, 12.9, and 13.1 GHz with the matching thickness of 1.3, 1.6, and 1.7 mm for CNFs-Fe, CNFs-Co, and CNFs-Ni, respectively. Among the three samples, CNFs-Fe has the most excellent EM-wave absorption properties with the thinnest matching thickness, similar to the MWCNTs/Fe/Co/Ni nanopowder systems.⁶ This may be ascribed to the fact that CNFs-Fe has the highest permeability resulting from its largest saturation magnetization. For comparison, we also investigate

the absorption properties of the silicone composites with 5 wt% pure CNFs in the 1–18 GHz range, as shown in Figure 11d. However, the pure CNFs sample gives a very weak EM absorption compared with the CNFs-*M* composites, and the minimum RL value only reaches –11.5 dB, which is mainly attributed to the poor impedance matching between the material and free space due to its high permittivity at 1–18 GHz ($\epsilon' = 70.0\text{--}15.1$, $\epsilon'' = 57.5\text{--}18.5$).

The thickness of the sample is one of the crucial parameters which affects the intensity and the position of the frequency at the RL minimum.⁵⁰ As can be clearly seen in Fig. 11, the absorption peaks shift to lower frequency and peak values show a tendency of first decrease and then increase with increasing thickness from 1.1 to 5.0 mm for all samples, implying that the absorption performances can

be effectively and easily tuned through adjusting the thickness of the composites. Additionally, it is interesting to noting that when the sample thickness exceeds 3.0 mm for CNFs-Fe or 4.0 mm for CNFs-Co and CNFs-Ni, a second absorption peak appears after the main peak, which is beneficial to improve the effective absorbing bandwidth of a single absorber layer. According to the quarter-wavelength cancellation model, the minimal reflections can be obtained at given frequency if the thickness of the absorber satisfies $d = nc/(4f\sqrt{|\epsilon_r||\mu_r|})$ ($n = 1, 3, 5, \dots$).^{6,21} Hence, the attenuation peaks move toward the lower frequency regions and more attenuation peaks might appear as the thickness of the absorbers increases.

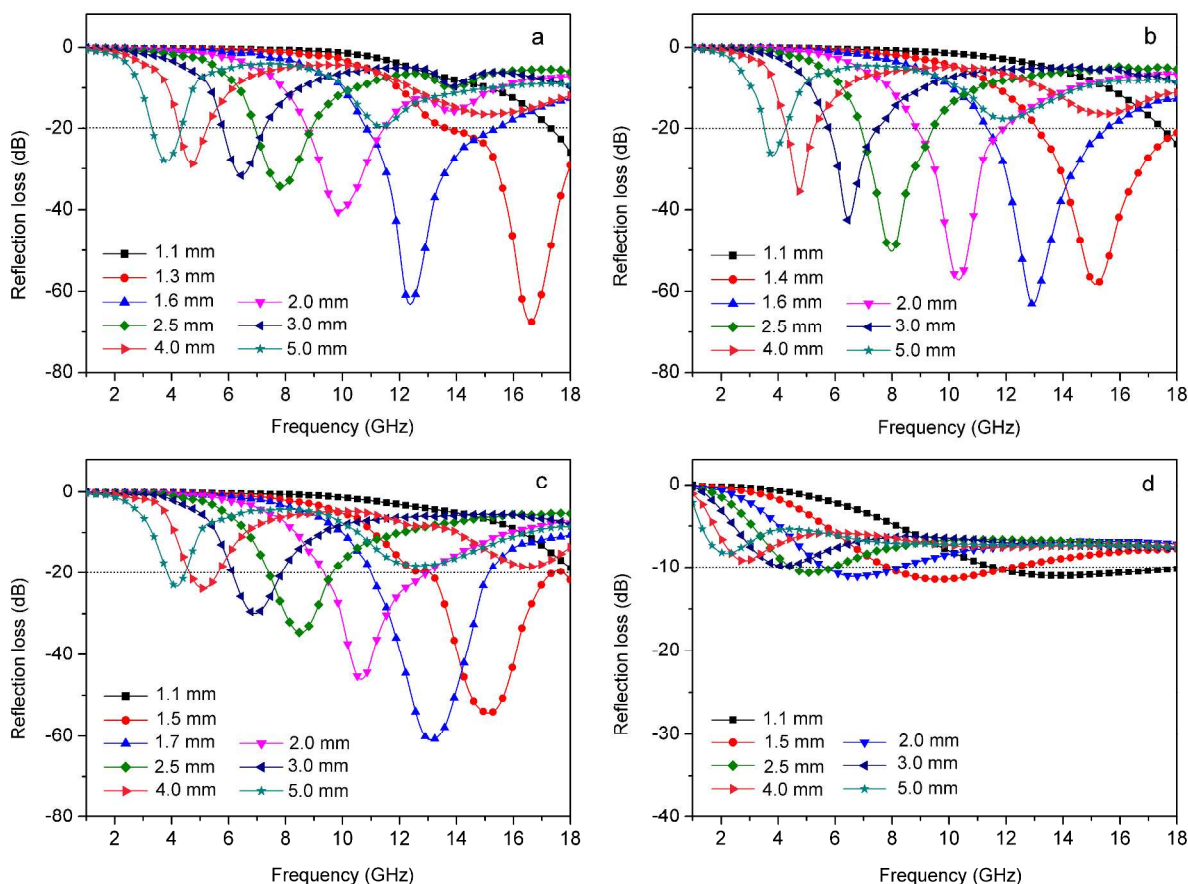


Fig. 11 Reflection loss curves of (a) CNFs-Fe, (b) CNFs-Co, (c) CNFs-Ni, and (d) CNFs/silicone composites with different thicknesses in the frequency range of 1–18 GHz.

As shown in Table 1, the EM-wave absorption properties of the present CNFs-*M* systems are compared with other magnetic carbon hybrid nanocomposites reported recently.^{6,8,13,20–22,25,31,40,44,51–55} It can be seen that the CNFs-Fe, CNFs-Co, and CNFs-Ni have stronger EM absorbing ability and broader absorption bandwidth at a lower mass density and a thinner absorber layer. Generally, excellent EM absorption performance of a material requires good impedance matching and attenuation characteristics, which are associated with complex permittivity, complex permeability, thickness, and structure of the material.^{21,44,49} For the CNFs-*M* fabricated in the present work, their dielectric and magnetic loss, especially for magnetic loss, are not high compared to other reported magnetic carbon hybrid absorbers listed in Table 1. Therefore,

one can conclude that the enhancement of the EM-wave absorption properties for the three samples may be mainly contributed to a better electromagnetic impedance matching which is set up due to their relatively low permittivity and special core/shell microstructures. As a result, the input impedance of the CNFs-*M* composites is closer to the wave impedance of free space, more energy of the incident EM-waves can be transferred and dissipated inside the absorbers, leading to a stronger and wider EM absorption. Besides, it should be herein emphasized that an important feature of the present work is that the mass fraction of CNFs-*M* in the silicone composites is only 5 wt%. In other words, the areal density of absorbers is mainly dominated by the matrix materials not by the fillers. These results show that as-prepared CNFs/*M* hybrid

nanofibers are very promising to be used as stable, lightweight and highly efficient EM-wave absorptive materials in a wide frequency range.

Table 1 EM-wave absorption properties of some earlier reported magnetic carbon hybrid nanocomposites.

sample	Mass ratio (wt%)	Absorber thickness (RL < -20dB) (mm)	Frequency range (RL < -20dB) (GHz)	Minimum RL		Ref.
				Value (dB)	Matching thickness (mm)	
CoNi/C nanocapsules	40	2.0–4.8	~5–17	-35	2.0	[13]
Ni/C nanocapsules	50	2.0	12.5–13.5	-32	2.0	[31]
FeNi/C nanocapsules	40	2.0–3.0	9–18	-22.5	2.0	[40]
Prous C/Co	30	~2.5–5.0	~4–10	-40	5.0	[44]
Fe ₃ O ₄ /C composite nanofibers	5	5.0	~7.3–8.7	-45	5.0	[8]
Fe-Co/carbon fibers	30	1.5–3.0	5.7–12.5	-48.2	1.7	[20]
Fe ₃ O ₄ /carbon fibers	50	1.7–6.0	2–8.5	-30	4.0	[21]
CuO/carbon fibers	50	1.5–4.0	3.0–9.4	-29.6	1.8	[22]
Fe-C nanofibers	50	2.0–3.5	~3.5–7.2	-44	3.0	[25]
MWCNTs/Fe	60	3.36–5.57	2.04–3.47	-39	4.27	[6]
MWCNTs/Co	60	4.18–6.82	2.35–3.51	-37	5.25	[6]
FeCo/CNTs	30	~6.0–10.0	~9–15.5	-37.3	8.0	[51]
Ni/MWCNTs	30	2.7–5.3	4.7–10.2	-37.9	4.0	[52]
Fe ₃ O ₄ /MWCNTs	20	2.0–5.0	~4.6–18	-75	3.0	[53]
Fe/graphene	40	1.5–4.0	~4.8–18	-45	3.0	[54]
NiFe ₂ O ₄ nanorod/graphene	60	2.0–5.0	~5.7–18	-44.6	4.0	[55]
CNFs/Fe	5	1.1–5.0	3.3–18	-67.5	1.3	This work
CNFs/Co	5	1.1–5.0	3.5–18	-63.1	1.6	This work
CNFs/Ni	5	1.1–5.0	3.8–18	-61.0	1.7	This work

Conclusions

In summary, electrospinning combined with heat treatment in Ar atmosphere has been employed to successfully prepare the magnetic carbon nanofibers CNFs-*M* in which the in-situ formed magnetic metal (Fe, Co, and Ni) nanoparticles are uniformly dispersed along nanofibers and encapsulated by ordered graphite layers. The formed core-shell microstructure can improve the impedance matching, EM-wave absorption properties and oxidation and corrosion resistances of the metal nanoparticles in CNFs-*M*. The magnetism and EM-wave absorption analysis show that RL values exceeding -20 dB are obtained in the frequency range of 3.3–18, 3.5–18, and 3.8–18 GHz with the absorber thickness between 1.1 and 5.0 mm for the silicone composites containing 5 wt% CNFs-Fe, CNFs-Co, and CNFs-Ni as fillers, respectively. The effectively absorbing frequency range covers the absorption frequency range of the traditional sintered ferrites and many earlier reported nanocomposites. Moreover, the RL minimums respectively reach -67.5, -63.1, and -61.0 dB at 16.6, 12.9, and 13.1 GHz with the matching thickness of 1.3, 1.6, and 1.7 mm. As a result, the as-synthesized CNFs-*M* hybrid nanofibers have a wide absorption frequency range, strong absorption ability, low density, and good physical and chemical stability, which are very attractive for potential applications in EM-wave absorbing materials.

Acknowledgements

This work is financially supported by the National Natural Science Foundation of China (51274106 and 11204108), China Postdoctoral Science Foundation (2013M510418), Science and Technology Support Program of Jiangsu Province (BE2012143

and BE2013071), Natural Science Foundation of the Jiangsu Higher Education Institutions of China (11KJB430006 and 12KJA430001), and Jiangsu Planned Projects for Postdoctoral Research Funds (1301055B).

Notes and references

^a School of Mathematics and physics, Jiangsu University of Science and Technology, Zhenjiang 212003, People's Republic of China. E-mail: jxiang@just.edu.cn; Fax: +86-511-84401171; Tel: +86-511-84401171

^b Institute of Advanced Materials, Jiangsu University, Zhenjiang 212013, People's Republic of China

- Z. Han, D. Li, H. Wang, X. G. Liu, J. Li, D. Y. Geng and Z. D. Zhang, *Appl. Phys. Lett.*, 2009, 95, 023114.
- K. Y. Park, J. H. Han, S. B. Lee, J. B. Kim, J. W. Yi and S. K. Lee, *Compos. Sci. Technol.*, 2009, 69, 1271.
- X. Huang, M. Lu, X. Zhang, G. Wen, Y. Zhou and L. Fei, *Scripta Mater.*, 2012, 67, 613.
- B. Wen, X. X. Wang, W. Q. Cao, H. L. Shi, M. M. Lu, G. Wang, H. B. Jin, W. Z. Wang, J. Yuan and M. S. Cao, *Nanoscale*, 2014, 6, 5754.
- Y. C. Qing, W. C. Zhou, F. Luo and D. M. Zhu, *Carbon*, 2010, 48, 4074.
- F. S. Wen, F. Zhang and Z. Y. Liu, *J. Phys. Chem. C*, 2011, 115, 14025.
- P. F. Guan, X. F. Zhang and J. J. Guo, *Appl. Phys. Lett.*, 2012, 101, 153108.
- T. Zhang, D. Q. Huang, Y. Yang, F. Y. Kang and J. L. Gu, *Mater. Sci. Eng. B*, 2013, 178, 1.
- Q. L. Liu, B. Cao, C. L. Feng, W. Zhang, S. M. Zhu and D. Zhang, *Compos. Sci. Technol.*, 2012, 72, 1632.
- Z. J. Wang, L. N. Wu, J. G. Zhou, W. Cai, B. Z. Shen and Z. H. Jiang, *J. Phys. Chem. C*, 2013, 117, 5446.
- X. Sun, J. P. He, G. X. Li, J. Tang, T. Wang, Y. X. Guo and H. R. Xue, *J. Mater. Chem. C*, 2013, 1, 765.
- C. G. Hu, Z. Y. Mou, G. W. Lu, N. Chen, Z. L. Dong, M. J. Hu and L. T. Qu, *Phys. Chem. Chem. Phys.*, 2013, 15, 13038.

- 13 H. Wang, Y. Y. Dai, W. J. Gong, D. Y. Geng, S. Ma, D. Li, W. Liu and Z. D. Zhang, *Appl. Phys. Lett.*, 2013, 102, 223113.
- 14 R. Kumar Srivastava, T. N. Narayanan, A. P. Reena Mary, M. R. Anantharaman, S. Srivastava, R. Vajtai and P. M. Ajayan, *Appl. Phys. Lett.*, 2011, 99, 113116.
- 15 K. Y. Park, J. H. Han, S. B. Lee and J. W. Yi, *Compos. Part A*, 2011, 42, 573.
- 16 G. Li, T. S. Xie, S. L. Yang, J. H. Jin and J. M. Jiang, *J. Phys. Chem. C*, 2012, 116, 9196.
- 17 Y. Liu, Z. Q. Zhang, S. T. Xiao, C. W. Qiang, L. L. Tian and J. C. Xu, *Appl. Surf. Sci.*, 2011, 257, 7678.
- 18 C. W. Qiang, J. C. Xu, Z. Q. Zhang, L. L. Tian, S. T. Xiao, Y. Liu and P. Xu, *J. Alloys Compd.*, 2010, 506, 93.
- 19 I. M. D. Rosa, A. Dinescu, F. Sarasini, M. S. Sarto and A. Tamburrano, *Compos. Sci. Technol.*, 2010, 70, 102.
- 20 L. Wang, F. He and Y. Z. Wan, *J. Alloys Compd.*, 2011, 509, 4726.
- 21 X. G. Meng, Y. Z. Wan, Q. Y. Li, J. Wang and H. L. Luo, *Appl. Surf. Sci.*, 2011, 257, 10808.
- 22 J. Zeng, J. C. Xu, P. Tao and W. Hua, *J. Alloys Compd.*, 2009, 487, 304.
- 23 L. W. Ji, O. Toprakci, M. Alcoutlabi, Y. F. Yao, Y. Li, S. Zhang, B. K. Guo, Z. Lin and X. W. Zhang, *ACS Appl. Mater. Interfaces*, 2012, 4, 2672.
- 24 J. L. Zhang, J. C. Fu, F. S. Li, E. Q. Xie, D. S. Xue, N. J. Mellors and Y. Peng, *ACS Nano*, 2012, 6, 2273.
- 25 T. Wang, H. D. Wang, X. Chi, R. Li and J. B. Wang, *Carbon*, 2014, 74, 312.
- 26 N. A. M. Barakat, M. F. Abadir, K. T. Nam, A. M. Hamza, S. S. Al-Deyab, W. I. Baek and H. Y. Kim, *J. Mater. Chem.*, 2011, 21, 10957.
- 27 N. A. M. Barakat, B. Kim, S. J. Park, Y. Jo, M. H. Jung and H. Y. Kim, *J. Mater. Chem.*, 2009, 19, 7371.
- 28 L. Wang, Y. Yu, P. C. Chen and C. H. Chen, *Scripta Mater.*, 2008, 58, 405.
- 29 J. W. Ji, Z. Lin, A. J. Medford and X. W. Zhang, *Chem. Eur. J.*, 2009, 15, 10718.
- 30 J. R. Liu, M. Itoh and K. I. Machida, *Appl. Phys. Lett.*, 2006, 88, 062503.
- 31 X. F. Zhang, X. L. Dong, H. Huang, Y. Y. Liu, W. N. Wang, X. G. Zhu, B. Lv, J. P. Lei and C. G. Lee, *Appl. Phys. Lett.*, 2006, 89, 053115.
- 32 D. K. Kim, S. H. Park, B. C. Kim, B. D. Chin, S. M. Jo and D. Y. Kim, *Macromol. Res.*, 2005, 13, 521.
- 33 S. H. Park, S. M. Jo, D. Y. Kim, W. S. Lee and B. C. Kim, *Synth. Met.*, 2005, 150, 265.
- 34 B. Wen, J. J. Zhao, T. J. Li, C. Dong and J. Z. Jin, *J. Phys.: Condens. Matter*, 2005, 17, L513.
- 35 I. Martin-Gullon, J. Vera, J. A. Conesa, J. L. González and C. Merino, *Carbon*, 2006, 44, 1572.
- 36 R. C. Che, C. Y. Zhi, C. Y. Liang and X. G. Zhou, *Appl. Phys. Lett.*, 2006, 88, 033105.
- 37 H. Wu, R. Zhang, X. X. Liu, D. D. Lin and W. Pan, *Chem. Mater.*, 2007, 19, 3506.
- 38 R. C. Che, L. M. Peng, X. F. Duan, Q. Chen and X. L. Liang, *Adv. Mater.*, 2004, 16, 401.
- 39 S. Ramo, J. R. Whinnery and T. V. Duzer, *Fields and Waves in Communication Electronics*, Wiley, New York, 1984.
- 40 X. G. Liu, Z. Q. Qu, D. Y. Geng, Z. Han, J. J. Jiang, W. Liu and Z. D. Zhang, *Carbon*, 2010, 48, 891.
- 41 C. Kittel, *Phys. Rev.*, 1948, 73, 155.
- 42 A. Aharoni, *J. Appl. Phys.*, 1991, 69, 7762.
- 43 L. J. Deng and M. G. Han, *Appl. Phys. Lett.*, 2007, 91, 023119.
- 44 Q. L. Liu, D. Zhang and T. X. Fan, *Appl. Phys. Lett.*, 2008, 93, 013110.
- 45 Y. J. Chen, F. Zhang, G. G. Zhao, X. Y. Fang, H. B. Jin, P. Gao, C. L. Zhu, M. S. Cao and G. Xiao, *J. Phys. Chem. C*, 2010, 114, 9239.
- 46 B. Wen, M. S. Cao, M. M. Lu, W. Q. Cao, H. L. Shi, J. Liu, X. X. Wang, H. B. Jin, X. Y. Fang, W. Z. Wang and J. Yuan, *Adv. Mater.*, 2014, 26, 3484.
- 47 B. Wen, M. S. Cao, Z. L. Hou, W. L. Song, L. Zhang, M. M. Lu, H. B. Jin, X. Y. Fang, W. Z. Wang and J. Yuan, *Carbon*, 2013, 65, 124.
- 48 Y. J. Chen, G. Xiao, T. S. Wang, Q. Y. Ouyang, L. H. Qi, Y. Ma, P. Cao, C. L. Zhu, M. S. Cao and H. B. Jin, *J. Phys. Chem. C*, 2011, 115, 13603.
- 49 B. Lu, H. Huang, X. L. Dong, X. F. Zhang, J. P. Lei, J. P. Sun and C. Dong, *J. Appl. Phys.*, 2008, 104, 114313.
- 50 G. B. Sun, B. X. Dong, M. H. Cao, B. Q. Wei and C. W. Hu, *Chem. Mater.*, 2011, 23, 1587.
- 51 Z. Han, D. Li, X. W. Wang and Z. D. Zhang, *J. Appl. Phys.*, 2011, 109, 07A301.
- 52 G. X. Tong, F. T. Liu, W. H. Wu, F. F. Du and J. G. Guan, *J. Mater. Chem. A*, 2014, 2, 7373.
- 53 M. S. Cao, J. Yang, W. L. Song, D. Q. Zhang, B. Wen, H. B. Jin, Z. L. Hou and J. Yuan, *ACS Appl. Mater. Interfaces*, 2012, 4, 6949.
- 54 X. C. Zhao, Z. M. Zhang, L. Y. Wang, K. Xi, Q. Q. Cao, D. H. Wang, Y. Yang and Y. W. Du, *Sci. Rep.*, 2013, 3, 3421.
- 55 M. Fu, Q. Z. Jiao and Y. Zhao, *J. Mater. Chem. A*, 2013, 1, 5577.

Graphical Abstract

Magnetic carbon nanofibers containing uniformly dispersed Fe/Co/Ni nanoparticles (CNFs-*M*) exhibit excellent electromagnetic wave absorption properties from C-band to Ku-band.

